# Determination of light-scattering form factors of latex particle dimers with simultaneous static and dynamic light scattering in an aggregating suspension

Helmut Holthoff,[1] Michal Borkovec,[1,*] and Peter Schurtenberger[2]
[1]*Institut für Terrestrische Ökologie, Eidgenössische Technische Hochschule Zürich, Grabenstrasse 3, 8952 Schlieren, Switzerland*
[2]*Institut für Polymere, Eidgenössische Technische Hochschule Zürich, 8092 Zürich, Switzerland*
(Received 28 July 1996)

Light-scattering form factors and hydrodynamic radii of latex particle dimers were obtained by time-resolved experiments in aggregating suspensions of latex particles with radii of 155 and 290 nm. The method relies on a simultaneous measurement of static and dynamic light scattering at different angles with a fiber-optics-based multiangle instrument in the early stages of the aggregation, where only particle dimers are formed. Combined analysis of such simultaneous experiments allows the determination of absolute coagulation rate constants without reference to light-scattering and hydrodynamic properties of the dimers. The knowledge of this rate constant permits the evaluation of the dimer form factors from the static or the dynamic experiment. The experimentally determined form factors agree well with results of calculation based on modal analysis and discrete dipole approximation. [S1063-651X(97)13311-6]

PACS number(s): 82.70.Dd, 42.25.Fx, 78.35.+c, 83.70.Hq

## I. INTRODUCTION

Various phenomena in colloid science can be investigated by light-scattering techniques. However, in most cases, the analysis requires the knowledge of light-scattering properties, such as, for instance, the light-scattering form factor of the particles. Until recently, few theories were available for light-scattering form factors of clusters and aggregates, whereby these theories were restricted to small particle sizes and simply shaped particles. Meanwhile, these restrictions could be overcome to a large extent and these efforts resulted in a number of approaches for the theoretical investigation of light scattering from aggregates.

One general method for computing scattering and absorption by particles of arbitrary shape is the discrete dipole approximation (DDA) [1,2] developed by DeVoe, Purcell, and Pennypacker [3–5]. In this method the solid particles are replaced by an array of point dipoles, where the spacing between the dipoles is small compared to the wavelength. The dipoles interact with the incident field as well as with the electric fields due to all of the other dipoles in the array. The coupled linear equations describing the dipole polarization are solved by iterative methods.

Another approach that is appropriate for calculating form factors of clusters and aggregates is the modal analysis. Thereby the incident and scattered fields are expanded in a convenient basis set, whose symmetry is commensurable with the geometry of the scatterer. The method relies on the so-called addition theorems, which enable the transformation of the basis functions from the coordinate origin of one monomer to another. One reason for the relatively late development of this theory for aggregates consisting of spherical monomers is the fact that the necessary addition theorems for spheres were only derived in the early 1950s [6–8]. Most efficient schemes rely on the superposition formulation, in which the total solution for the field outside the particles is constructed from the superposition of the individual solutions of each monomer [9–16].

Such theories are potentially very interesting in various applications that involve scattering of light from aggregates in the micrometer size range. For example, they are important in atmospheric sciences to understand the optical properties of aerosols and dust particle aggregates, or in colloid science to address light-scattering properties of aggregates of larger or optically dense particles. Such theories, however, have not yet been tested systematically in the optical regime; available tests were carried out with microwaves on macroscopically large spheres [17,18].

The aim of the present study is to provide an independent examination of the validity of these theories in the optical regime. In the following, we shall discuss experimental determination of dimer form factors in an aggregating colloidal suspension in an aqueous electrolyte solution. In the early stages of the aggregation, only particle doublets are formed and their optical properties can be determined by monitoring the light-scattering signals in a time-resolved experiment. The experiments were performed on a fiber-optics-based multiangle instrument, which permits the simultaneous measurement of static and dynamic light scattering at different angles [19–21].

## II. THEORY

### A. Light scattering

The most frequently used light-scattering theory for the description of the form factor of aggregates is the classical Rayleigh-Gans-Debye (RGD) approach, which provides simple analytical expressions. The main idea behind the RGD approximation is the concept of independent subscatterers. The whole volume of the scattering object is subdivided into many volume elements. Each element represents a Rayleigh scatterer that is excited by the incident wave. Due to the assumption that each volume element scatters indepen-

*Author to whom correspondence should be addressed.

 

dently from the rest of the particle, no interference between the waves occurs inside the particle, or more mathematically spoken, the field inside the particle is approximated by the incident field.

Within the RGD approximation, the form factor of a spherical particle is given by [22,23]

$$P_1(q)=\frac{9}{(qa)^6}[\sin(qa)-(qa)\cos(qa)]^2, \qquad (2.1)$$

where $a$ is the radius of the primary particle and $q=(4\pi/\lambda)\sin(\theta/2)$ is the magnitude of the scattering vector with $\theta$ being the scattering angle and $\lambda$ the wavelength of the light in the medium. The general expression of the form factor of an arbitrary aggregate of spherical particles can be written within the RGD approximation as a sum over all pairs of particle centers in the aggregates [22,24]

$$P_z(q)=\frac{P_1(q)}{z^2}\left[\sum_{i,j}\frac{\sin(r_{ij}q)}{(r_{ij}q)}\right], \qquad (2.2)$$

where $z$ is the number of spheres within the aggregate and $r_{ij}$ is the center-to-center distance between particles $i$ and $j$.

The consequence of the RDG approximation is that the intensity of the scattered light depends only on the spatial arrangement of the volume elements and one assumes that the incident wave does not undergo any changes in the phase or amplitude after entering the particle. This condition leads to the following regime of validity of the RDG approximation:

$$\frac{2\pi L}{\lambda}|m-1|\ll 1, \qquad (2.3)$$

where $L$ is the longest linear dimension of the particle and $\lambda$ is the wavelength of the light in the medium and $m$ is the ratio of the complex refractive index of the particle relative to the refractive index of the surrounding medium. Therefore, the simple analytical RGD expression is valid for particles of arbitrary shape only if the particle size and the refractive index are not too large. For the case of latex particles in aqueous suspension, this limitation prevents the use of this approach for particles $\lesssim 250$ nm in diameter.

In order to overcome the size limitation of the RGD theory it is necessary to allow for phase and amplitude changes of electromagnetic waves within the particles. The exact solution of this problem for a single sphere due to Mie is straightforward and is readily available [22,25]. However, the solution of the analogous problem for aggregates of spheres is nontrivial, and solutions of this problem were given only recently [1–5,12–16]. The problem can be approached with two different techniques: (i) the discrete dipole approximation (DDA), which is a numerical method for solving scattering problems for objects of arbitrary shape, and (ii) modal analysis (MA), which permits an analytical solution of the scattering problem for an aggregate of spheres.

In the DDA the scatterer is divided into identical elements, where each element, arranged, for instance, on a cubic lattice, is small enough to be represented by a dipole oscillator. The polarizability of each element is chosen such that the bulk dielectric function is obtained when inserted into the Clausius-Mossotti relation [5]. This relation connects the microscopic polarizability to the macroscopic bulk dielectric function of the particle material. Because the classical Clausius-Mosotti relation applies in the long wavelength limit only, a corresponding lattice dispersion relation must be considered [1,26].

Each dipole located at $\mathbf{r}_j$ has an oscillating polarization $\mathbf{P}_j=\alpha_j\mathbf{E}_j$ where $\mathbf{E}_j$ is the electric field at its location, which is driven by both the incident field $\mathbf{E}_{\mathrm{inc},j}$ and the electric field of all the other dipoles in the array. This coupling of all scattering elements within the particle leads to a set of coupled linear equations,

$$\sum_k \mathbf{A}_{jk}\mathbf{P}_k=\mathbf{E}_{\mathrm{inc},j}, \qquad (2.4)$$

where the summation runs over all dipoles within the array and the symmetric matrix $\mathbf{A}_{jk}$ is related to the polarizabilities along the diagonal by $\mathbf{A}_{jj}=1/\alpha_j$ while the off-diagonal elements represent the coupling between the individual dipoles. This linear system of equations can be solved numerically. The total scattered field is then determined by the summation of all the dipole fields, and the far-field limit of the scattered electric field can be evaluated as

$$\mathbf{E}_{\mathrm{sca}}(\mathbf{r})=\frac{k^2e^{ikr}}{r}\sum_j e^{-ik\hat{\mathbf{r}}\cdot\mathbf{r}_j}(\hat{\mathbf{r}}\hat{\mathbf{r}}-\mathbf{I})\mathbf{P}_j, \qquad (2.5)$$

where $k=2\pi/\lambda$ is the magnitude of the incident wave vector, $\hat{\mathbf{r}}=\mathbf{r}/r$ a unit vector and $\mathbf{I}$ the unit $3\times 3$ matrix. This method is applicable to any particle geometry. However, one must ensure that the spacing between the dipoles is small compared to the wavelength of a plane wave in the target material, and that the number of dipoles is large enough to describe the target shape satisfactorily. The optimum discretization grid is determined by varying the number of discretization grid points and by comparison of the results with analytical solutions for spheres. Since light-scattering form factors involve orientational averaging, the calculations must be usually repeated for different orientations, which makes this method computationally expensive.

The MA appears to be the most efficient way to solve the multiple sphere scattering problem. The field of the incident wave $\mathbf{E}_{\mathrm{inc}}$ and the scattered wave $\mathbf{E}_{\mathrm{sca}}$ is expanded in basis functions, whose symmetry is commensurable with the geometry of the scatterer. The total solution of the external field outside the cluster is then constructed from the superposition of the individual solutions of each monomer.

For a collection of spherical particles the incident and scattered fields can be decomposed into individual fields of each sphere $j$, which in turn are expanded into vector spherical harmonics [23]

$$\mathbf{E}^j_{\mathrm{inc}}(\mathbf{r}^j)=\sum_{n,m}[a^j_{mn}\mathbf{M}^{(1)}_{mn}(q\mathbf{r}^j)+b^j_{mn}\mathbf{N}^{(1)}_{mn}(q\mathbf{r}^j)], \qquad (2.6)$$

$$\mathbf{E}^j_{\mathrm{sca}}(\mathbf{r}^j)=\sum_{n,m}[p^j_{mn}\mathbf{M}^{(3)}_{mn}(q\mathbf{r}^j)+q^j_{mn}\mathbf{N}^{(3)}_{mn}(q\mathbf{r}^j)], \qquad (2.7)$$

where $\mathbf{r}^j$ originates at the center of sphere $j$; the expansion coefficients for the incident and scattered fields are $(a^j_{mn}, b^j_{mn})$ and $(p^j_{mn}, q^j_{mn})$, respectively. The vector spherical harmonics $\mathbf{M}^{(1)}_{mn}$ and $\mathbf{N}^{(1)}_{mn}$ have a Bessel-function radial dependence and are regular at the origin, whereas $\mathbf{M}^{(3)}_{mn}$ and $\mathbf{N}^{(3)}_{mn}$ have a radial dependence based on the Hankel functions and vanish at infinity [27]. Due to the linearity of the Maxwell equations the relation between the column of the expansion coefficient of the incident plane wave $\mathbf{a}^j=(a^j_{mn}, b^j_{mn})$ and those of the initially unknown scattered field $\mathbf{p}^j=(p^j_{mn}, q^j_{mn})$, can be expressed by a system of linear equations in matrix form

$$\mathbf{a}^j+\sum_{j,j'}\mathbf{T}^{jj'}\mathbf{a}^{j'}=\mathbf{p}^j, \tag{2.8}$$

where $\mathbf{T}^{jj'}$ represents transition matrices, which transform the expansion coefficients of the incident field into the corresponding coefficients of the scattered field. The matrix elements $\mathbf{T}^{jj'}$ are obtained by means of addition theorems for spherical vector harmonics. The most efficient method for the solution of Eq. (2.8) is the ''order of scattering'' technique [14,15]. This technique is an iterative scheme, which is based upon the concept of multiple reflection. The external field about a given monomer is composed of a series of partial fields arising from first, second, and higher reflections of neighboring spheres plus the incident field. Additional refinements of these techniques are discussed elsewhere [16].

### B. Combined evaluation and hydrodynamic theories

Consider the very early stages of aggregation in a dilute, initially monomeric particle suspension. For sufficiently short times only the monomers and particle doublets dominate and the presence of all higher order aggregates can be neglected [28–30]. In this regime, the concentration evolution can be described according to

$$\frac{dN_1}{dt}=-kN_1^2, \tag{2.9}$$

$$\frac{dN_2}{dt}=\frac{1}{2}kN_1^2, \tag{2.10}$$

where $N_1(t)$ and $N_2(t)$ are the number concentrations of particle monomers and particle doublets, respectively. As long as one has contributions from the monomers and dimers only, the intensity of scattered light is given by

$$I(q,t)=I_1(q)N_1(t)+I_2(q)N_2(t), \tag{2.11}$$

where $I_1(q)$ and $I_2(q)$ are the scattered intensities from the monomers and doublets, respectively. Note that these quantities are directly related to the corresponding form factors by $P_1(q)=I_1(q)/I_1(0)$ and $P_2(q)=I_2(q)/I_2(0)$. Solving Eq. (2.9) for short times, the initial rate of change in the static light intensity can be expressed as

$$\frac{1}{I(q,0)}\left[\frac{dI(q,t)}{dt}\right]_{t\to 0}=kN_0\left[\frac{I_2(q)}{2I_1(q)}-1\right], \tag{2.12}$$

where $N_0$ is the initial particle concentration.

In the dynamic light-scattering experiment one can monitor the intensity averaged diffusion coefficient, which is obtained from the first cumulant of the field autocorrelation function and reads

$$D_{\mathrm{av}}(q,t)=\frac{D_1I_1(q)N_1(t)+D_2I_2(q)N_2(t)}{I_1(q)N_1(t)+I_2(q)N_2(t)}, \tag{2.13}$$

where $D_1$ and $D_2$ are the diffusion coefficients of the monomers and doublets, respectively. Using the solution of Eq. (2.9) and introducing the hydrodynamic radius $r_h$ by means of the Stokes-Einstein relation, one obtains for short times

$$\frac{1}{r_h(q,0)}\left[\frac{dr_h(q,t)}{dt}\right]_{t\to 0}=kN_0\left(1-\frac{r_{h,1}}{r_{h,2}}\right)\frac{I_2(q)}{2I_1(q)}, \tag{2.14}$$

where $r_{h,1}/r_{h,2}=D_2/D_1$ is the ratio of the hydrodynamic radii of the monomers and doublets.

Since the static and dynamic light-scattering signals can be measured simultaneously, the data can be analyzed in the following fashion. Eliminating the optical factor $I_2(q)/[2I_1(q)]$ from Eqs. (2.12) and (2.14) leads to a linear relation between two experimentally accessible quantities:

$$\frac{1}{I(q,0)}\left[\frac{dI(q,t)}{dt}\right]_{t\to 0}=\left(1-\frac{r_{h,1}}{r_{h,2}}\right)^{-1}\times\left\{\frac{1}{r_h(q,0)}\left[\frac{dr_h(q,t)}{dt}\right]_{t\to 0}\right\}-kN_0. \tag{2.15}$$

A straight line is obtained by plotting the initial rate of change of the static light-scattering intensity as a function of the corresponding quantity for the hydrodynamic radius. From its intercept the absolute coagulation rate constant follows, and from the slope we obtain the ratio of the hydrodynamic radii of the dimer and the monomer. Thus, simultaneous dynamic and static light-scattering measurements allow one to determine the absolute coagulation rate without any reference to light-scattering and hydrodynamic theories.

As additional information from these experiments, one obtains the ratio of the hydrodynamic radii of the doublet and the monomer $r_{h,2}/r_{h,1}$. The ratio can be evaluated from different theories in a low Reynolds number fluid [31]. The hydrodynamic radius is related by the Stokes-Einstein relation to the mutual diffusion coefficients, which can be expressed in terms of the resistance coefficients of the two spheres along $\lambda_{\parallel}(R)$ and perpendicular $\lambda_{\perp}(R)$ to their line of centers by

$$D(R)=\frac{k_BT}{6\pi\eta r}\mathrm{tr}\frac{1}{2}\begin{pmatrix}\lambda_{\parallel}^{-1}(R) & 0 & 0\\ 0 & \lambda_{\perp}^{-1}(R) & 0\\ 0 & 0 & \lambda_{\perp}^{-1}(R)\end{pmatrix}, \tag{2.16}$$

where $k_B$ is the Boltzmann constant, $T$ is the absolute temperature, $\eta$ is the viscosity of the fluid, $R$ is the distance between the centers of the two spheres and tr is the trace. For

the case where the two spheres touch ($R=2a$) and are not free to rotate, one obtains $\lambda_{\parallel}^{-1}(2a)=0.645$ and $\lambda_{\perp}^{-1}(2a)\simeq 0.694$ [32]. The ratio of the hydrodynamic radii of the doublet and the monomer turns out to be

$$r_{h,2}/r_{h,1}\simeq 1.38. \tag{2.17}$$

If the two spheres are free to rotate $r_{h,2}/r_{h,1}\simeq 1.35$.

The hydrodynamic radii can be also obtained by means of the probabilistic path method. In this method the friction coefficients are calculated from hitting probabilities of random walks launched from a spherical surface, which encloses the object of interest [33]. In the case of a doublet of two fixed spheres this method $r_{h,2}/r_{h,1}=1.396\pm 0.009$. In the Kirkwood-Risemann approximation the friction coefficient of an aggregate composed of identical particles is estimated only by the number of particles and their center-to-center distances [34–36]. This approximation gives for the same situation, $r_{h,2}/r_{h,1}\simeq 1.33$.

## III. EXPERIMENT

### A. Material

Two different types of polystyrene latex particles were used. The first polystyrene latex was manufactured by Interfacial Dynamics Corporation, Portland (IDC) without the use of surfactants. According to the information provided by IDC, the particles have a radius of 155 nm with a coefficient of variation of 2.8% as measured by electron microscopy. They are charge stabilized by carboxyl groups with a surface charge density of 9.0 $\mu$C/cm$^2$. The stock solution has a concentration of $2.58\times 10^{18}$ m$^{-3}$.

The second latex was prepared at Granada University according to a standard emulsifier-free polymerization method using potassium persulphate as initiator [37]. The obtained raw latex particles, which are stabilized by sulfate groups, were cleaned by serum replacement and ion exchange over a mixed bed. Electron microscopy was employed to determine the particle radius and its coefficient of variation to be 290 nm and 4.7%, respectively. The surface charge density is 2.4 $\mu$C/cm$^2$ [20]. The particle concentration in the stock suspension is $6.37\times 10^{17}$ m$^{-3}$. Experiments with aggregating suspensions were performed in 1.0*M* KCl electrolyte solution and at a temperature of 25 °C. Stable suspensions were prepared in 1m*M* KCl. The water for the electrolyte and latex solution was taken from a Millipore ion exchange apparatus.

### B. Setup

The measurements were performed on a fiber-optics-based multiangle instrument, where static and dynamic light scattering are performed simultaneously. Details for this device and its performance are given elsewhere [21]. Using single and few mode fibers from OZ Optics and photomultiplier tubes from Hamamatsu (H3460-54) the scattered light is simultaneously collected at nine fixed angles between 13° to 134°. Two ALV-5000 correlator boards, which can record two independent correlation functions with 128 channels each, were used to perform dynamic light-scattering measurement at four angles simultaneously. As the light source an argon ion laser (Coherent Innova 200-10) operating at a wavelength of 488 nm is employed.

A computer-controlled multiplexer selects the photomultiplier signals that are being sent to the correlators. One can therefore choose the angles at which the dynamic measurements are being performed, which is particularly useful for many short time-resolved measurements as in the study of coagulation processes. It allows us to alternate between different groups of angles and thus to obtain a quasicontinuous series of dynamic light-scattering experiments at eight scattering angles with a temporal resolution of a few seconds. For an individual static and dynamic light-scattering measurement, data were typically accumulated for 10 s for a single measurement. Such measurements were repeated continuously in a time interval of 40 min up to several hours [19]. By changing the direction of the incident beam relative to the optical axis, a continuous range of scattering angles can be obtained [21]. This enables a complete angular scan in the static and dynamic light-scattering measurements of the time-dependent coagulation process.

### C. Combined evaluation

For the 155-nm particles the final latex concentration in the cell was in the range from $6.6\times 10^{13}$ m$^{-3}$ up to $1.2\times 10^{14}$ m$^{-3}$. For the 290 nm particles all measurements were made with a concentration of $N_0\simeq 4.0\times 10^{13}$ m$^{-3}$. Although the measurements are in the fast coagulation regime these particle concentrations ensure a half-time of about 4000 s, which allows one to study the initial dimer formation without measurable contributions of triplets and larger aggregates to the light scattering intensity. The coagulation half time is the time where the total particle concentration is reduced by a factor of two. Further details can be found in Ref. [19].

The coagulation rate constants of the latices were determined by combined evaluation of the simultaneously measured static and dynamic light scattering data [Eq. (2.15)]. The change in the static light scattering $I(q,0)^{-1}[dI(q,t)/dt]_{t\to 0}$ as a function of the dynamic light scattering $r_h(0)^{-1}[dr_h(t)/dt]_{t\to 0}$ at the same $q$ value leads to a linear relationship. The intercept of this curve contains the information about the rate constants and the slope is determined by the hydrodynamic factor $(1-r_{h,1}/r_{h,2})^{-1}$ from which the hydrodynamic radius of the dimer particles can be determined. Therefore, both parameters can be obtained from the fit with no *a priori* knowledge of the light scattering or the hydrodynamic properties of the particles.

The linear plots used to determine the absolute coagulation rate constants are shown in Fig. 1 for the 155 nm and the 290 nm particles. For the fast coagulation rate constant, we obtain $k=(2.4\pm 0.4)\times 10^{-18}$ m$^3$ s$^{-1}$ in the case of the 155 nm particles and $k=(6.9\pm 0.6)\times 10^{-18}$ m$^3$ s$^{-1}$ in the case of the 290 nm particles.

### D. Static light scattering

Reflection and background corrections of the setup were determined from static light-scattering experiments on stable latex particle suspensions. The results were analyzed with a nonlinear fitting procedure, which involves the form factors of monomers based on the Mie theory [25] averaged over a

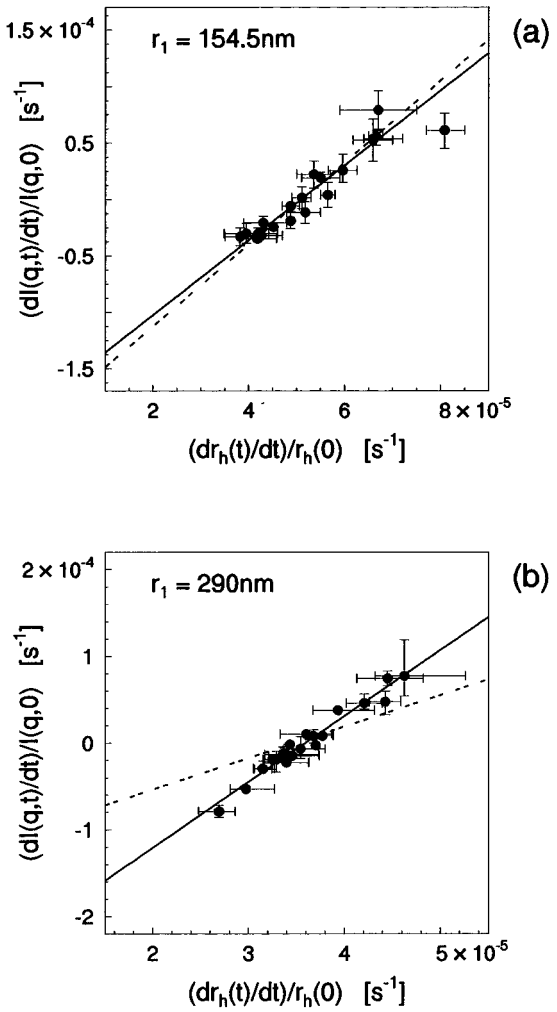


FIG. 1. Initial rate of change of the static light-scattering intensity $I(q,0)^{-1}[dI(q,t)/dt]_{t\to 0}$ is plotted vs the initial rate of change of the hydrodynamic radius $r_h(q,0)^{-1}[dr_h(q,t)/dt]_{t\to 0}$. The solid line is the best linear regression fit and the dashed line the expected linear relation for the theoretical values of the hydrodynamic radius $r_2/r_1=1.38$. Particle radius (a) 155 nm and (b) 290 nm.

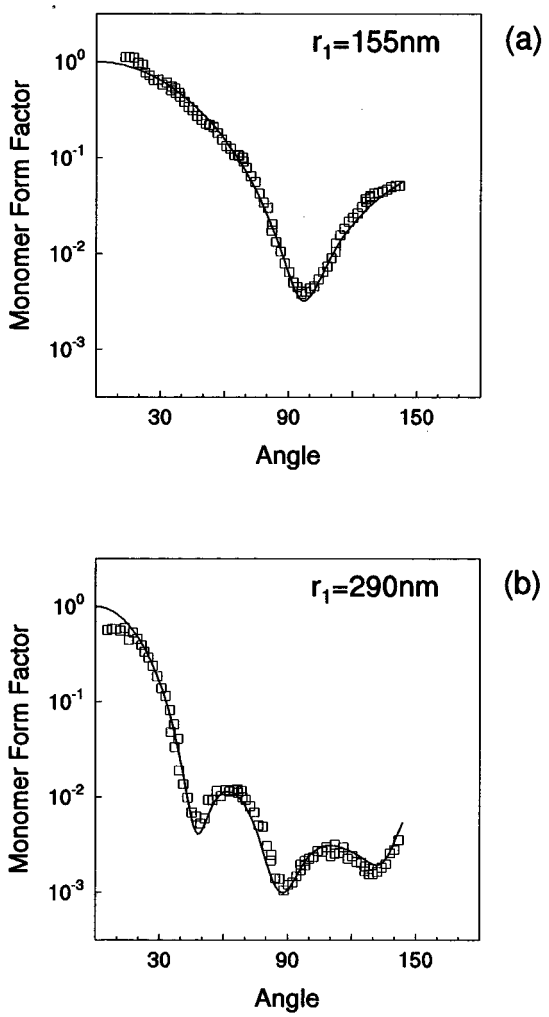


FIG. 2. Monomer form factor (dimensionless) plotted as a function of scattering angle (degrees). The experimental data (symbols) were measured in a stable suspension and are compared with the best fit using Mie theory for a polydisperse mixture of spheres (solid line). Particle radius (a) 155 nm and (b) 290 nm.

Gaussian distribution of polydisperse spheres. In order to obtain a quantitative description of the experimental data, it was necessary to introduce a reflectivity correction of the form

$$I'(\theta)=I(\theta)+2\rho^2 I(180°-\theta), \tag{3.1}$$

where $I'(\theta)$ and $I(\theta)$ are the corrected and uncorrected scattering intensities as a function of the scattering angle $\theta$ and $\rho$ is the reflection coefficient of the interface between the colloidal suspension and the scattering cell. The reflection correction has two equal contributions. The first contribution comes from the reflected primary beam from the front side of the light-scattering cell. This reflected beam also induces scattering into the detector. The second contribution originates from the scattered light, which is reflected on the opposite side of the detector. All other reflection contributions are of higher order.

The best fit results are compared with experimental data in Fig. 2 for both types of particles. Polystyrene has a refractive index of 1.596 and very weak absorption in the optical regime. In water we thus obtain a real refractive index ratio of $m\simeq 1.20$. For the smaller latex, the fitted radii and polydispersities are 155 nm and 3.0%. These values compare favorably with the corresponding results from TEM being 155 nm and 2.8%. For the larger latex, from static light scattering we obtain for the corresponding values 291 nm and 3.8%. These values are also in satisfactory agreement with TEM, which gives 290 nm and 4.7%. The fitted reflection coefficient turns out to be $\rho=0.19\pm 0.02$ in both cases. This value is significantly larger than the theoretical reflection coefficient of $\sim 0.06$ for a water-glass interface. The larger experimental reflection coefficient is not surprising since the fiber-optics-based multiangle instrument was not designed to minimize residual stray light and the beam stop of the primary beam may still cause some additional backreflection.

## IV. RESULTS AND DISCUSSION

### A. Dimer form factor

As described in the methods section, a combined evaluation of the static and dynamic light-scattering data allows the determination of the coagulation rate constant independent of any light-scattering and hydrodynamic theories for the dimer. Based on the rate constant determined in this way, the quantity $I_2(q)/[2I_1(q)] \propto P_2(q)/P_1(q)$ can be evaluated by using either Eq. (2.12) for the static light scattering or Eq. (2.14) for the dynamic light scattering. For the dynamic measurements [cf. Eq. (2.14)], the hydrodynamic factor $r_{h,1}/r_{h,2}$ has to be considered, which is determined from the experiments. Together with the experimentally determined form factors of the monomers $P_1(q)$, the form factor of the dimers $P_2(q)$ can be measured, in principle, up to a multiplicative constant. This constant corresponds to the ratio of the scattering powers for the doublet and the monomer $I_2(0)/[2I_1(0)]$. However, for the systems investigated the experimentally accessible quantity $I_2(q)/[2I_1(q)]$ oscillates as a function of $q$ and its extrapolation to $q \to 0$ is very difficult. In practice, therefore, the constant $I_2(0)/[2I_1(0)]$ cannot be measured with acceptable accuracy and the doublet form factor $P_2(q)$ can only be determined up to an unknown proportionality constant.

The experimental results for the doublet form factors $P_2(q)$ are compared with the prediction based on the modal analysis including polydispersity (MAP) in Fig. 3 for both particle sizes. The unknown proportionality constant was adjusted for optimal overlap between experimental data and theory. One observes no systematic discrepancies between the form factors obtained by static or dynamic light-scattering measurements. This means that the angular dependence of both signals is governed by the same factor and the coincidence between both detection methods provides an independent confirmation of the present analysis. The theoretical prediction was calculated using the MA, which includes averaging over all possible doublets taken from independent Gaussian distributions with the appropriate polydispersity. The reflectivity correction was incorporated using Eq. (3.1) and the reflectivity coefficient taken from the appropriate measurements of the monomers. The agreement between theory and experiment for the 155 nm particles is very good, while for the 290 nm particle the agreement is inferior but still satisfactory. In the Appendix it is shown that the presently developed analysis can be simply extended to the polydisperse situation by using the form factors averaged over the size distribution of the particles.

Figure 4 compares various theoretical predictions of the doublet form factors. The doublet form factor calculated by modal analysis including polydispersity (MAP), which was shown in Fig. 3, is now displayed without the reflectivity correction. One observes some effects of the polydispersity, as revealed by comparing with the result of the modal analysis for a monodisperse sample (MAM). The latter calculation was verified with the discrete dipole approximation. In this calculation, each sphere was discretized into $32 \times 32 \times 32$ elements into each direction. The results obtained from MAM and DDA agree rather well. Comparable agreement between these two methods was reported previously [38]. Clearly, the classical RDG approximation fails in this regime entirely.

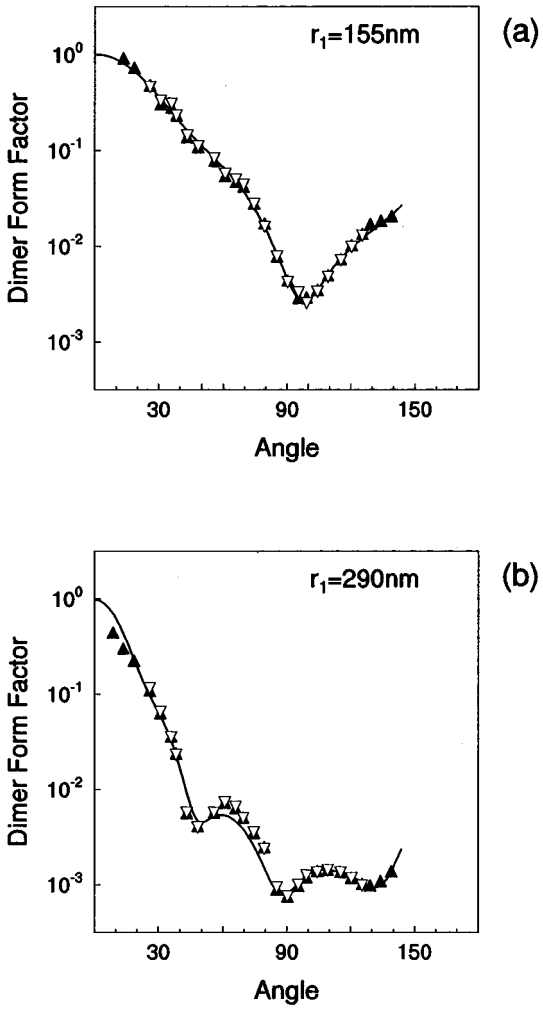


FIG. 3. Dimer form factor (dimensionless) plotted as a function of scattering angle (degrees). The experimental data are derived from static (▲) and dynamic (▽) light-scattering experiments in the early stages of an aggregating suspension. Solid line is the calculation based on modal analysis including polydispersity (MAP). Particle radius (a) 155 nm and (b) 290 nm.

### B. Dimer hydrodynamic radius

Following Eq. (2.15) the hydrodynamic radius of the dimer particles can be obtained from the slope of the linear fit. In Fig. 1(a) the experimentally determined dimer radius for the smaller latex particles $r_{h,2}/r_{h,1} = 1.43 \pm 0.09$ is compared with the theoretical prediction of $r_{h,2}/r_{h,1}$ (dotted line), which was calculated by the method of reflection [31] and turns out to be $r_{h,2} \simeq 1.38 \times r_{h,1}$, if the two spheres are not free to rotate. Discrepancies to the theoretical predictions are more pronounced in the case of the 290 nm particles, where we find $r_{h,2}/r_{h,1} = 1.15 \pm 0.02$ with a error much smaller than the error of the hydrodynamic ratio for the 155 nm particles. Therefore, only the value for the larger particles differs significantly from the theoretical radius ratio, whereas this theoretical value is within the error interval for the smaller particles. This trend, agreement between the theoretical and experimental hydrodynamic dimer radii for small particles, and disagreement for larger particles, was already observed earlier for 215 nm sulfate latex [19] and 683 nm sulfate latex

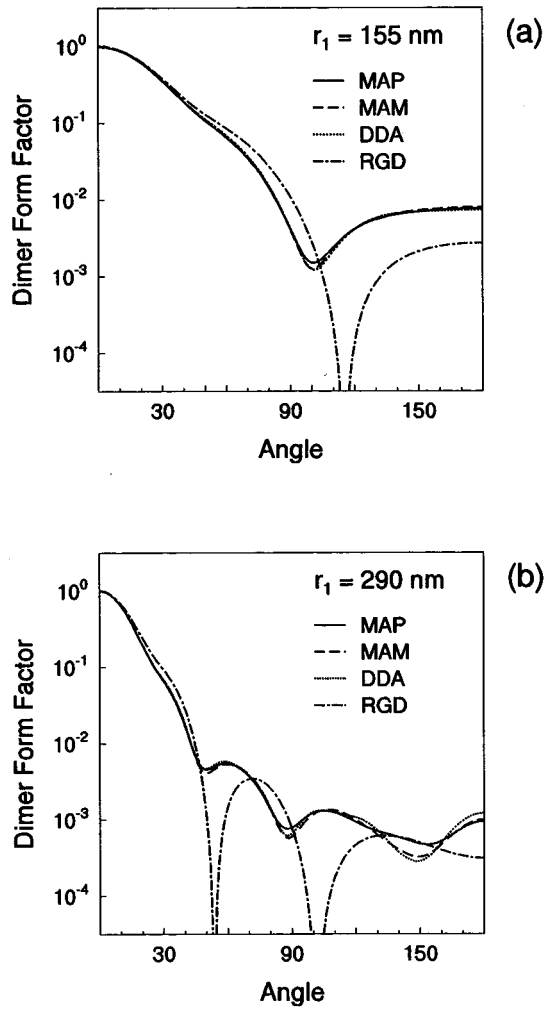


FIG. 4. Various calculated dimer form factors (dimensionless) plotted as a function of the scattering angle (degrees). The modal analysis including polydispersity (MAP) is compared with the results of the modal analysis for a monodisperse suspension (MAM). The latter result is very close to the calculation based on discrete dipole approximation. All these form factors deviate substantially from the Rayleigh-Gans-Debye theory. Particle radius (a) 155 nm and (b) 290 nm.

[20]. From the theoretical point of view the hydrodynamic radius ratio should be independent of the particle size, and no satisfactory explanation of this discrepancy could be found so far.

## V. CONCLUSION

Time-resolved simultaneous static and dynamic light-scattering experiments in aggregating suspensions enable us to determine the form factor of dimers from submicron latex particles. The experimentally determined dimer form factors were compared with theoretical predictions of this quantity. Such predictions were based on the modal analysis for the polydisperse (MAP) and monodisperse situation (MAM). The modal analysis of monodisperse particle doublets was cross-checked using the discrete dipole approximation. The experimental observations were in satisfactory agreement with the theoretical predictions for both particle sizes examined. The present results thus confirm the appropriateness of recent computational schemes of the scattering of electromagnetic radiation in the optical regime.

## ACKNOWLEDGMENTS

We gratefully acknowledge B. Draine and M. Mackowski for providing us with their computer programs and G. Koper for helpful discussions. One of the employed lattices was kindly supplied by A. Schmitt and R. Hidalgo-Álvarez from the University of Granada. This study was supported by the Swiss National Science Foundation.

## APPENDIX

For a polydisperse suspension of primary particles, the evolution of the monomer and dimer particles at the early stage of the coagulation process can be described by the evolution equation

$$\frac{dN_1(r,t)}{dt} = -\int_0^\infty k(r,r')N_1(r,t)N_1(r',t)\,dr', \quad \text{(A1)}$$

$$\frac{dN_2(r,r',t)}{dt} = \frac{1}{2}k(r,r')N(r,t)N(r',t), \quad \text{(A2)}$$

where $N(r,t)$ is the number density of monomers of radius $r$ at time $t$, $N(r,r',t)$ is the number density of dimers formed of monomers of radii $r$, $r'$, and $k(r,r')$ the coagulation rate constant of monomers of size $r$ and $r'$.

In a static light-scattering experiment, the scattered light intensity from a dilute polydisperse suspension is given by

$$I(q,t) = \int_0^\infty I_1(r,q)N_1(r,t)\,dr + \int_0^\infty \int_0^\infty I_2(r,r',q)N_2(r,r',t)\,dr\,dr', \quad \text{(A3)}$$

where $I_1(r,q)$ is the scattered intensity of a monomer of size $r$ and $I_2(r,r',q)$ the scattered intensity of a dimer composed of particles of size $r$ and $r'$.

Taking the derivative with respect to time, the initial change in the light scattering intensity can be expressed as

$$\frac{1}{I(q,0)}\left[\frac{dI(q,t)}{dt}\right]_{t\to 0} = \left[\int_0^\infty N_1(r,0)I_1(r,q)\,dr\right]^{-1}\left\{\int_0^\infty\int_0^\infty N_1(r,0)N_1(r',0)k(r,r')\left[\frac{I_2(r,r',q)}{2} - I_1(r,q)\right]dr\,dr'\right\}. \quad \text{(A4)}$$

This expression can be simplified for suspensions with low polydispersities as considered here. In this case, the distribution of the particles $N_1(r,0)$ is rather sharply peaked at the average radius $\overline{r}$. A slowly varying function inside the integral, such as

$k(r,r')$, can be approximated by a constant and evaluated at the average radius $\overline{r}$. On the other hand, a rapidly varying or oscillating function such as $I_1(r,q)$ or $I_2(r,r',q)$ must be kept inside the integral. Making this type of approximation, Eq. (A4) can be simplified to

$$\frac{1}{I(q,0)}\left[\frac{dI(q,t)}{dt}\right]_{t\to 0} \simeq \overline{k}N_0\left[\frac{\overline{I}_2(q)}{2\overline{I}_1(q)}-1\right], \tag{A5}$$

where $\overline{k}=k(\overline{r},\overline{r})$, $N_0=\int_0^\infty N_1(r,0)\,dr$ is the total number of monomers, while $\overline{I}_1(q)$ and $\overline{I}_2(q)$ are the number averaged scattering intensities of the monomers and doublets, respectively. These quantities are given by

$$\overline{I}_1(q)=\frac{1}{N_0}\int_0^\infty N_1(r,0)I_1(r,q)\,dr \tag{A6}$$

and

$$\overline{I}_2(q)=\frac{1}{N_0^2}\int_0^\infty\int_0^\infty N_1(r,0)N_1(r',0)I_2(r,r',q)\,dr\,dr'. \tag{A7}$$

Note that Eq. (A5) has precisely the same structure as Eq. (2.12) derived for a monodisperse suspension.

In the case of dynamic light scattering, the averaged diffusion coefficient determined from the first cumulant is given by

$$D_{av}(q,t)=\left[\int_0^\infty I_1(r,q)N_1(r,t)\,dr+\int_0^\infty\int_0^\infty I_2(r,r',q)N_2(r,r',t)\right]^{-1}\left[\int_0^\infty D_1(r)I_1(r,q)N_1(r,t)\,dr\right.$$
$$\left.+\int_0^\infty\int_0^\infty D_2(r,r')I_2(r,r',q)N_2(r,r',t)\,dr\,dr'\right], \tag{A8}$$

where $D_1(r)$ is the diffusion coefficient of monomer of size $r$ and $D_2(r,r')$ the diffusion coefficient of a dimer consisting of monomers of size $r$ and $r'$. Using the Stokes-Einstein relation for $D_{\mathrm{av}}(q)$ we obtain the initial rate of change of the hydrodynamic radius $r_h(q,t)$ by taking the time derivative of Eq. (A8):

$$\frac{1}{r_h(q,0)}\left[\frac{dr_h(q,t)}{dt}\right]_{t\to 0}=\left[\int_0^\infty N_1(r,0)D_1(r)I_1(r,q)\,dr\right]^{-1}\left\{\int_0^\infty\int_0^\infty N_1(r,0)N_1(r',0)k(r,r')\left[\frac{D_2(r,r')}{2}I_2(r,r',q)\right.\right.$$
$$\left.-D_1(r)I_1(r,q)\right]dr\,dr'\Bigg\}-\left[\int_0^\infty N_1(r,0)I_1(r,q)\,dr\right]^{-1}\left\{\int_0^\infty\int_0^\infty N_1(r,0)N_1(r',0)k(r,r')\right.$$
$$\left.\times\left[\frac{1}{2}I_2(r,r',q)-I_1(r,q)\right]dr\,dr'\right\}. \tag{A9}$$

The same argument, which has led us from Eq. (A4) to Eq. (A5), can be applied to Eq. (A9). Thereby, we observe that in addition to the function $k(r,r')$ the functions $D_2(r,r')$ and $D_1(r)$ are slowly varying as well. In this case, we obtain

$$\frac{1}{r_h(q,0)}\left[\frac{dr_h(q,t)}{dt}\right]_{t\to 0}\simeq\overline{k}N_0\left(\frac{\overline{r}_{h,1}}{\overline{r}_{h,2}}-1\right)\frac{\overline{I}_2(q)}{2\overline{I}_1(q)}, \tag{A10}$$

where $\overline{r}_{h,1}/\overline{r}_{h,2}=D_2(\overline{r},\overline{r})/D_1(\overline{r})$ and all other quantities were defined above. Again, Eq. (A10) has the same structure as its analog Eq. (2.14) derived for a monodisperse suspension.

Equations (A5) and (A10) govern the initial changes of the static and dynamic light-scattering signals for an aggregating suspension of particles with a small but finite polydispersity. In these equations, the polydispersity effect enters only through the number averaged optical factors $\overline{I}_1(q)$ and $\overline{I}_2(q)$. Thus both modes of detection allow the determination of the same quantities. The agreement between these two results in the polydisperse situation provides a further indication of the correctness of the analysis given.

[1] B. T. Draine, Astrophys. J. **333**, 848 (1988).
[2] B. T. Draine and P. J. Flatau, J. Opt. Soc. Am. A **11**, 1491 (1994).
[3] H. DeVoe, J. Chem. Phys. **41**, 393 (1964).
[4] H. DeVoe, J. Chem. Phys. **43**, 3199 (1965).
[5] E. M. Purcell and C. R. Pennypacker, Astrophys. J. **186**, 705 (1973).
[6] B. Friedman and J. Russek, Q. Appl. Math. **12**, 13 (1954).
[7] S. Stein, Q. Appl. Math. **19**, 15 (1961).
[8] O. R. Cruzan, Q. Appl. Math. **20**, 33 (1962).
[9] C. Liang and Y. T. Lo, Radio Sci. **2**, 1481 (1967).
[10] J. H. Brunning and Y. T. Lo, IEEE Trans. Antennas Propag. **19**, 378 (1971).
[11] J. H. Brunning and Y. T. Lo, IEEE Trans. Antennas Propag. **19**, 391 (1971).
[12] F. Borghese, P. Denti, G. Toscano, and O. I. Sindoni, Appl. Opt. **18**, 116 (1979).
[13] F. Borghese, P. Denti, G. Toscano, and O. I. Sindoni, J. Opt. Soc. Am. A **1**, 183 (1984).
[14] K. A. Fuller and G. W. Kattawar, Opt. Lett. **13**, 90 (1988).
[15] K. A. Fuller and G. W. Kattawar, Opt. Lett. **13**, 1063 (1988).
[16] D. W. Mackowski, Proc. R. Soc. London, Ser. A **433**, 599 (1991).
[17] R. T. Wang, J. M. Greenberg, and D. W. Schuerman, Opt. Lett. **6**, 543 (1981).
[18] K. A. Fuller, G. W. Kattawar, and R. T. Wang, Appl. Opt. **25**, 2521 (1986).
[19] H. Holthoff, S. U. Egelhaaf, M. Borkovec, P. Schurtenberger, and H. Sticher, Langmuir **12**, 5541 (1996).
[20] H. Holthoff, A. Schmitt, A. Fernández-Barbero, M. Borkovec, M. Cabrerizo-Vílchez, P. Schurtenberger, and R. Hidalgo-Álvarez, J. Colloid Interface Sci. **192**, 463 (1997).
[21] S. U. Egelhaaf and P. Schurtenberger, Rev. Sci. Instrum. **67**, 2 (1996).
[22] M. Kerker, *The Light Scattering of Light and Other Electromagnetic Radiation* (Academic Press, New York, 1969).
[23] C. F. Bohren and D. R. Huffman, *Adsorption and Scattering of Light by Small Particles* (Wiley, New York, 1983).
[24] G. Oster and D. P. Riley, Acta Crystallogr. **5**, 1 (1952).
[25] P. W. Barber and S. C. Hill, *Light Scattering by Particles: Computational Methods* (World Scientific, Singapore, 1990).
[26] B. T. Draine and J. Goodman, Astrophys. J. **405**, 685 (1993).
[27] M. Abramowitz and I. A. Stegun, *Handbook of Mathematical Functions* (Dover, New York, 1964).
[28] M. von Smoluchowski, Phys. Z. **17**, 557 (1916).
[29] M. von Smoluchowski, Z. Phys. Chem. (Munich) **92**, 129 (1917).
[30] M. L. Broide and R. J. Cohen, J. Colloid Interface Sci. **137**, 350 (1990).
[31] J. Happel and H. Brenner, *Low Reynolds Number Hydrodynamics* (Martinus Nijhoff Publishers, The Hague, 1983).
[32] In the direction along the line of the two spheres the value from the exact solution for two spheres is taken instead of the calculated value from the method of reflection.
[33] J. F. Douglas, H.-X. Zhou, and J. B. Hubbard, Phys. Rev. E **49**, 5319 (1994).
[34] J. G. Kirkwood and J. Risemann, J. Chem. Phys. **16**, 565 (1948).
[35] J. G. de la Torre and V. A. Bloomfield, Q. Rev. Biophys. **14**, 139 (1981).
[36] J. G. de la Torre, S. Navarro, M. C. L. Martinez, F. G. Diaz, and J. J. L. Cascales, Biophys. J. **67**, 530 (1994).
[37] J. W. Goodwin, J. Hearn, C. C. Ho, and R. H. Ottewill, Colloid Polym. Sci. **252**, 464 (1974).
[38] P. J. Flatau, K. A. Fuller, and D. A. Mackowski, Appl. Opt. **32**, 3302 (1993).